CHEMISTRY & SUSTAINABILITY

CHEMSUSCHEM

ENERGY & MATERIALS

Accepted Article

Title: Role of heteroatoms in S, N-codoped nanoporous carbons in CO2 (photo)electrochemical reduction

Authors: Teresa Bandosz and Wanlu Li

To be cited as: *ChemSusChem* 10.1002/cssc.201801073

Link to VoR: http://dx.doi.org/10.1002/cssc.201801073

A Journal of

ChemPubSoc Europe

WILEY-VCH

www.chemsuschem.org

Role of heteroatoms in S, N-codoped nanoporous carbons in CO_2 (photo)electrochemical reduction

Dr. Wanlu Li, and Prof. Teresa J. Bandosz*

Department of Chemistry and Biochemistry, The City College of New York, New York, NY 10031, USA, and Ph.D. Program in Chemistry, The Graduate Center of the City University of New York, New York, NY 10016, USA

* Whom correspondence should be addressed to: Tel; (212) 650-607; Fax: (212) 650-6107; *tbandosz@ccny.cuny.edu*

Abstract

Thiourea-modified wood-based activated carbons were evaluated as catalysts for CO_2 electrochemical reduction reaction (CO_2ERR). The materials obtained at 950^{o}C showed a long stability. The results indicated that thiophenic sulfur provides catalytic activity for CO formation. However, it was not as active for CH_4 formation as was pyridinic-N. Tafel plots suggested that the nanoporous structure enhanced the kinetics for CO_2 reduction. The electric conductivity limited the activity for CO_2ERR in the materials modified at 600, 800 and 900^{o}C. The effect of visible light on CO_2ERR was also investigated in this study. Upon irradiation, photocurrent was generated, and a current density increased during CO_2 reduction process. Combined with a band-gap alignment, the results indicate that thiophenic-S in the carbon matrix contributed to sample's photoactivity in visible light. These species enhance the overall reduction process promoting both hydrogen evolution reaction and CO_2 reduction to CO.

Introduction

The rising concentration of CO_2 in the atmosphere becomes an environmental issue, which leads to the global climate change. It also results in an increased ocean acidification affecting many marine ecosystems. Especially it is detrimental for the creatures with calcium carbonate in their shells or skeleton. One of the way to decrease/eliminate these effects is CO_2 electrochemical reduction. It emerged as a potential strategy for achieving a carbon-neutral cycle. The key challenge for this application is to develop selective, stable, efficient and inexpensive electrocatalysts. Metal-free nitrogen-doped carbon nanotube,[1–5] nanofibers[6], nanowires[7], graphene[8,9] and carbon frameworks[10] have been studied in recent years as catalysts for the electrochemical CO_2 reduction. It has been reported that CO is formed on N-doped carbon nanofibers and N-doped carbon nanotubes (NCNTs).[1-4] Formate is another desired product and Wang and co-workers[8] reported that the Faradaic efficiency (FE) for formate formation on N-doped graphene reached its maximum of 73% at −0.84 V vs. RHE. The catalyst indicated stability for 12 hours when tested at -0.84 V. It showed enhanced reduction reaction kinetics, increased selectivity and improved stability of N-graphenes during electrocatalysis in comparison to those measured on unmodified graphene oxides. It was also found that the pyridinic-N configuration provides catalytic activity. N-doped graphene quantum dots were also reported as highly active catalysts for a hydrocarbon and multi-carbon oxygenates formation when used as for CO_2ERR. They showed the total 90% FE for the reduction CO_2 process, which includes the 45% FE for the CO formation and the 45% of FE for the C_2 products (ethylene and ethanol) formation. It was concluded that the pyridinic-N groups at the edge site were more active to induce C–C bond formation than those at basal planes. This led to a higher yield of C_2 and C_3 products than those on N-doped graphene oxides materials.

Recently, porous carbons have gained attention as potential catalysts for the CO_2 electrochemical reduction (CO_2ERR). Song and coworkers[11] studied a series of mesoporous N-doped carbons with highly uniform cylindrical pore structures. The Faradaic efficiency for ethanol formation was 77% at -0.56 vs. RHE with a 6h stable performance. The cylindrical pore structure facilitated the dimerization of the key CO* intermediate resulting in the formation of ethanol. The DFT calculation suggested the both pyridinic-N and pyrrolic-N sites were the active sites for its formation. The C-C bond formation was more favorable at pyridinic-N sites than at pyrolic-N. Attempts were also made to explore CO_2 electroreduction on nanoporous carbon membranes to avoid an addition of any binder. Wang and coworkers[12] studied N-doped nanoporous carbon/carbon-nanotube composite membrane as binder-free electrodes for electrochemical reduction of CO_2. Hierarchically structured porous N-doped carbon membranes (HNCMs) provided a large surface area with incorporated active nitrogen species. CNTs were processed into a membrane to further improve an electron transfer efficiency. The composite showed the FE for the formate formation of 81% at -0.8V vs RHE and maintained it for 36 h without any decay in the performance. It is found that pyridinic-N was active and selective for the reduction process.

Wood-based N-doped nanoporous carbons as CO_2 electroreduction catalysts have been studied by our group.[13] The best sample showed the FE for CO and CH_4 formation of 24% and 0.76%, respectively. Besides, on the electrochemically reduced form of the carbon catalyst the FE for CO and CH_4 increased to 39 % and 1.2%, respectively. The results supported the previous finding indicating that pyridinic-N was the most active site for CO_2ERR among all the nitrogen-containing functional groups present on the surface of carbons. The surface basicity and a high volume of ultramicropores improved the CO_2 reduction process. There was an indication that a nanoporous structure is crucial for the CH_4 formation.[13] It was suggested that the ultramicropores work as

Fisher-Tropsch nanoreactors where methane is formed owing to a strong adsorption of CO* and an involvement of hydrogen from hydrogen evolution.

In another study molten salt synthesized N-doped carbons were used as CO_2 electrocatalysts. They showed a long stability (48h) with the FE for CO formation of 22%.[14] The results suggested that a unique pyrazinic-N species on the surface might act as sacrificial agents preventing the active site, especially pyridinic-N, from being oxidized during the reduction process. These species might also promote a C-C bond formation since C_3 products (acetone and propanol) were detected in the electrolyte.

Sulfur containing catalysts have seldom been tested for CO_2ERR. Metal-sulfur clusters have been studied around 30 years ago. The presence of the $[Fe_4S_4(SR)_4]^{2-}$ (R=$PhCH_2$ or Bu^t) cluster shifted 0.7V to a positive direction compared to a potential without the cluster on an mercury electrode in dimethylformamide (DMF) electrolyte.[15] The products were mainly formate and phenylacetate. The optimum efficiency for the formate formation was 27% on the $[Fe_4S_4(SCH_2Ph)_4]^{2-}$ cluster. $[M_2Fe_6S_8(SEt)_9]^{3-}$(M=Mo or W) also showed the 0.5V potential shift to the positive direction for the formate formation.[15] On rhodium cluster $[(RhCp^*)_3(u3\text{-}S)_2]^{2+}$ complex formate was detected at -1.5V vs SCE in the Bu_4NBF_4 containing CH_3CN electrolyte. Besides, in a $LiBF_4$ containing CH_3CN electrolyte, an oxalate formation was reported.[16] It was proposed that both low valent metals and electron rich sulfur ligands are the possible active sites for CO_2 reduction on the metal-sulfur clusters.

Recently, nitrogen and sulfur co-doped iron-containing highly porous carbon-gel has been studied for the CO_2 electroreduction reaction in an aqueous electrolyte.[17] CO was the main product and trace of methane was also detected. The catalyst showed the highest FE of 85% at -1.3V vs. RHE for CO. However, the role of sulfur in the CO_2ERR was not thoroughly discussed. Metal-free

sulfur containing nanoporous carbon has been tested in our previous study.[18] The Faradaic efficiency for the CO and CH_4 formation was only 2 and 0.1%, respectively. Even though the FE was very small, the XPS analysis suggested that the thiophenic-S was one of the activate sites for CO_2ERR. It is important to mention that sulfur-containing carbons have been reported as photocatalysts for various applications.[19–24] The sulfur in thiophenic configurations was indicated as the most crucial for photoactivity.[23] Therefore, it would be interesting to explore the effect of light on the electrochemical reduction of CO_2 on the sulfur-containing carbon catalysts.

The objective of the paper is to evaluate the role of sulfur species present in the microporous carbon matrix in the process of the CO_2 (photo) electroreduction. A series of microporous carbons containing both nitrogen and sulfur was prepared. The samples' porosity and surface chemistry were extensively examined. The trends in the catalytic behavior were analyzed and the role of various nitrogen and sulfur configurations, especially the latter species, was pointed out. Since photoactivity can be helpful for CO_2 reduction, the effect of visible light exposure on the samples' performance as CO_2 reduction catalysts has been also evaluated.

Results and discussion

The surface chemistry of the initial activated carbons was analyzed by X-ray photoelectron spectroscopy (XPS). As seen from Table 1, all BAX samples contain C, O, N and S. With an increase in the heating temperature the nitrogen and sulfur content decreased. While the content of sulfur decreased gradually, a dramatic drop in the content of nitrogen was found at 900^{o}C. Then the nitrogen content remained almost constant with further carbonization at 950^{o}C. Interestingly, the highest content of oxygen is in the sample heated at 800 ^{o}C, which indicates that this temperature results in the highest oxidation level of the BAX carbons modified with thiourea.

Table 1. Atomic concentration of elements on the surface determined by XPS analysis of the samples studied.*

Sample	(atomic %)			
	C	**O**	**N**	**S**
BAX-TU-600	82.8	8.2	5.8	3.2
BAX-TU-600-E	81.4	12.4	4.1	2.1
BAX-TU-800	81.2	13.0	3.6	2.2
BAX-TU-800-E	84.2	11.8	3.0	1.0
BAX-TU-900	88.3	8.8	1.3	1.6
BAX-TU-900-E	88.2	9.7	1.2	0.9
BAX-TU-950	86.6	10.7	1.5	1.2
BAX-TU-950-E	89.3	8.6	1.5	0.6

* The contribution from fluorine to the carbon 1s XPS spectrum has been subtracted.

The detailed deconvolution of C 1*s*, O 1*s*, N 1*s*, S *2p* core energy level spectra (Figure 1) revealed the differences in the specific configurations of the surface groups. Taking into account the deconvolution of C 1*s* core energy level spectra (Figure S1 of the Supporting Information, Table 2) and the atomic concentration (at. %) of carbon, the contribution of sp^2 carbon in BAX-600, 800, 900 and 950 are 60.9 at. %, 63.7 at. %, 67.0 at. %, 67.0 at. %. This suggests the number of carbon atoms involved in C-C bonds gradually increased with an increase in the carbonization temperature. For the sample heated to 950^{o}C, the amount of C-C bond remained the same at that in the sample heated to 900^{o}C, indicating similar carbonization level of the carbon matrices. Based on the deconvolution of O 1*s* core energy level spectra (Figure S1 of the Supporting Information, Table 2) and the surface elemental composition, and knowing that the contributions of O=C and C-O in BAX-TU-800 are similar to those in samples heated to 900^{o}C and 950^{o}C, the actual atomic concentration of the oxygen species on the BAX-TU-800 surface is higher than on those of other

samples. The marked contributions of carboxylic and carbonyl groups on this sample are expected to bring the acidic character to its surface.

The deconvolution of N 1*s* core energy level spectra (Table 2, Figure 1) revealed a transformation of nitrogen functionalities with an increase in the treatment temperature. The carbon heated at 600^{o}C showed mainly pyridinic (N-6) and pyrrolic (N-5) nitrogen. The treatment at 800^{o}C resulted in a decrease in the contribution of N-5 and the appearance of quaternary-N (N-Q) species. These results suggest that N-5 is converted to N-Q at 800^{o}C. Moreover, the ratio of the contributions of N-Q to N-6 increased from 0.36 at 800^{o}C to 3.2 at 950^{o}C indicating that N-6 is partially converted to N-Q at a high temperature. This process is accompanied by a significant loss of oxygen during heating, which was also reported from other studies on nitrogen containing carbons[25]. Both atomic concentration and relative concentration of pyridinic-N decreased with an increase in the heating temperature. Heating at 950^{o}C resulted also in the formation of N-oxides.[26]

10.1002/cssc.201801073

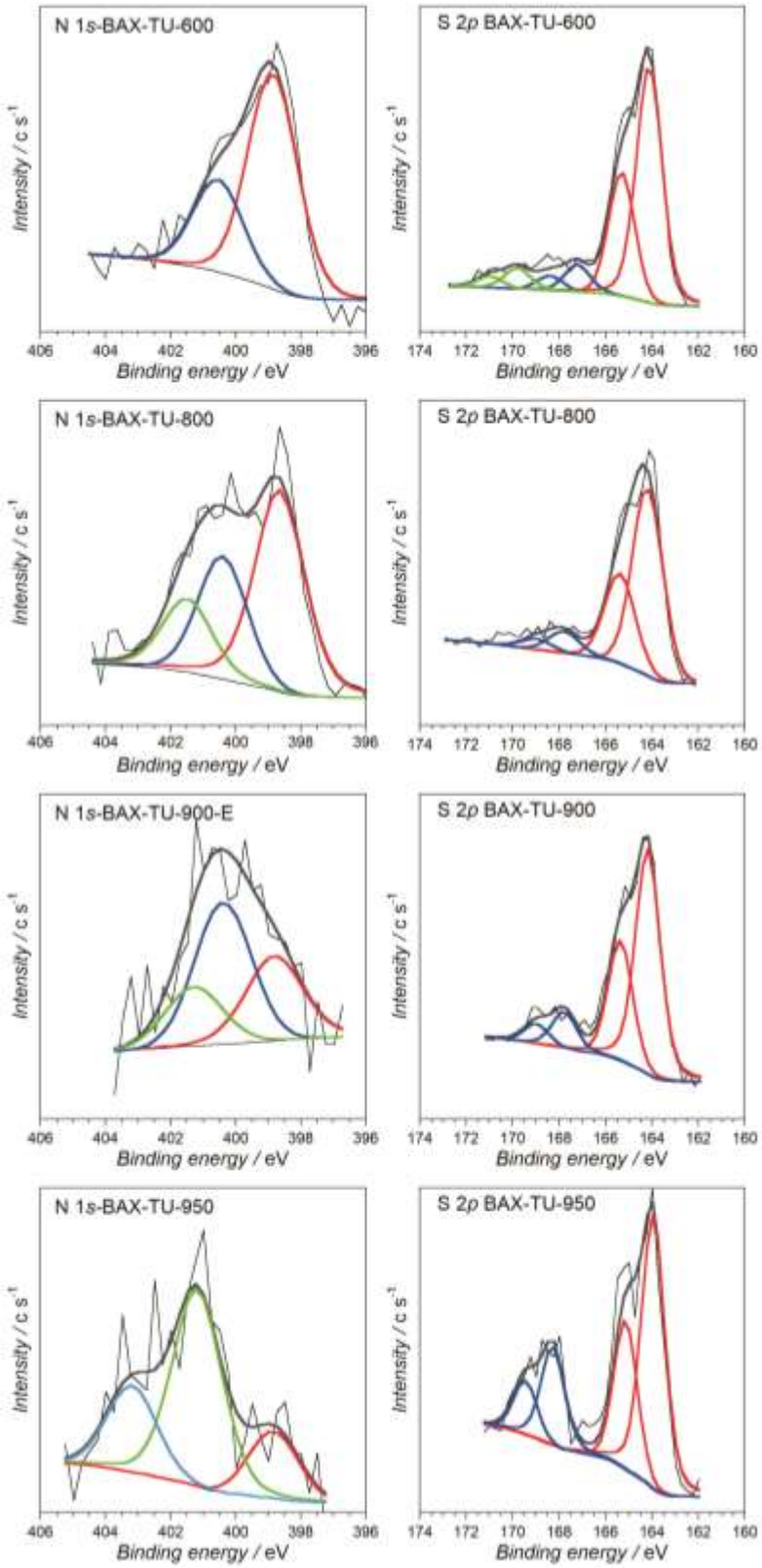

Figure 1. N 1*s* and S 2*p* core energy level spectra of the initial sample

Table 2. The results of deconvolution of C 1*s*, O 1*s*, N 1*s*, S *2p* core energy level spectra for the carbons studied.

	Energy, eV	Bond assignment	BAX-TU-600	BAX-TU-600-E	BAX-TU-800	BAX-TU-800-E	BAX-TU-900	BAX-TU-900-E	BAX-TU-950	BAX-TU-950-E
C 1s	284.7-284.8	C-C (sp^2, graphitic carbon)	73.5	80.8	78.5	73.3	75.9	77.2	77.4	66.7
	286.3-286.4	C-O, (in phenolic, alcoholic, etheric), C-N	16.4	17.5	15.2	24.1	15.5	19.8	14.0	31.5
	288.0-288.2	C=O (in carbonyl or quinone)	6.7	1.7	4.3	2.6	5.4	3.0	5.6	1.8
	289.6-290.1	O-C=O (in carboxyl or ester)	3.4		2.0		3.2		3.0	
O 1*s*	531.9-532.2	O=C (in carbonyl/ quinone) or O=S (in sulfoxides/ sulfones) or O=N	73.6	78.8	83.7	71.7	80.6	78.9	85.9	75.1
	533.4-533.8	O-C (in phenol/epoxy or O-S (in thioethers /sulfonic) or O-N	16.4	21.2	16.3	28.3	19.4	21.1	14.1	24.9
N 1*s*	398.7-398.8	N-6 (in pyridines)	70.0	52.8	52.0	27.0	39.1	31.3	18.0	18.3
	400.4-400.6	N-5 (in pyrroles)	30.0	47.2	29.0	50.0		47.7		70.8
	401.1-401.2	N-Q (in quaternary)			19.0	23.0	60.9	20.9	57.8	
	403.2	N-oxides							24.2	10.8
S $2p_{3/2}$	164.0-164.3	R-S-S-, C-S-C (in bisulfides/thiophenes)	82.1	56.7	88.7	73.9	85.9	61.8	73.4	57.1
	167.2-168.2	R_2-S=O (in sulfoxides) or R-SO_2 (in sulfones)	9.9	21.1	11.3	16.2	14.1	21.8	26.6	39.9
	169.8	R-SO_3H	8.0	22.2		9.9		16.4		11.0

The deconvolution of S 2*p* energy level spectra of the sample modified at 600°C (Table 2, Figure 1) indicates that the sulfur species on the surface are mainly in thophenic-S, sulfoxides (or sulfones) and sulfonic acid configurations. Further treatment at 800°C decreased the contribution of the latter two species. However, with the further increase in the heating temperature, the contribution of thiophenic-S decreased which was associated with an increase in the contribution of sulfoxides/sulfones.

The texture of the carbons has been also studied in detail. The parameters of the porous structure are presented in Table 3. All BAX carbons are micro/mesoporous with 62%-66% of the total pore volume existing in micropores. The impregnation with thiourea followed by heat treatment at various temperatures resulted in an alteration in the porous structures. Generally, an increase in the heating temperature led to a decrease in the surface area and total pore volume. Especially after heating at 950°C, the surface area and total volume decreased considerably. When the heating temperature reached 900°C and above, the microporous volume increased because of the partial gasification of the carbon and removal of the carbon atoms from the pore walls together with nitrogen, sulfur and oxygen atoms.

Table 3 also includes the conductivity of the carbon chips. The electric conductivity increased exponentially with an increase in the carbonization temperature, which is attributed to the transformation of disordered carbons to their higher order of aromaticity and condensation. Based on the contributions of C-C bonds from the XPS analysis, the sample heated at 600 and 800°C showed less carbon in the sp^2 configuration than those of 900 and 950°C, which is consistent with the lower conductivity of the former samples. The lower conductivity of the sample heated to 900°C in comparison to that heated at 950°C could be due to the higher sulfur content in the carbon matrix of the former sample. It is possible that the slight expansion of the d spacing in the carbon

matrix by sulfur decreases conductivity.[26] Both, the carbon in sp^2 configurations and surface chemistry affect the conductivity of the carbons.

Table 3. The parameters of the porous structure for the materials studied.

Sample	S_{BET} (m^2/g)	V_t (cm^3/g)	V_{meso} (cm^3/g)	$V_{<0.7\ nm}$ (cm^3/g)	$V_{<1\ nm}$ (cm^3/g)	V_{mic} (cm^3/g)	V_{mic}/V_t	Conductivity (S/m)
BAX-TU-600	1370	0.849	0.326	0.163	0.286	0.523	0.62	24±3
BAX-TU-800	1354	0.840	0.317	0.188	0.294	0.523	0.62	77±4
BAX-TU-900	1356	0.823	0.299	0.189	0.314	0.533	0.65	277±8
BAX-TU-950	1146	0.690	0.234	0.173	0.261	0.456	0.66	400±10

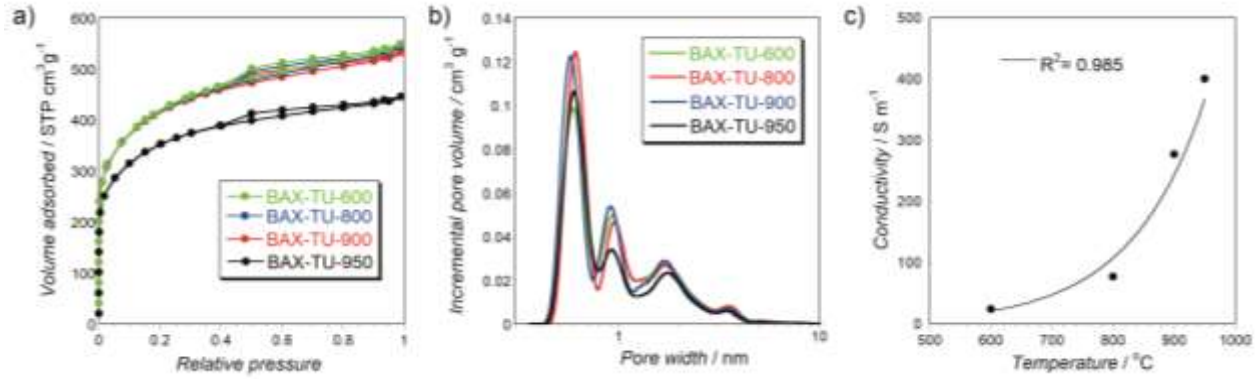

Figure 2. a) N_2 adsorption isotherms on the samples prepared at various temperatures; b) Pore size distributions; c) The relationship between the conductivity of the BAX-TU samples and the heat treatment.

The SEM and HR-TEM images revealed that our samples typical amorphous carbons from the view point of their microstructure. The examples of the images for BAX-TU-800 are included in Figure 3.

10.1002/cssc.201801073

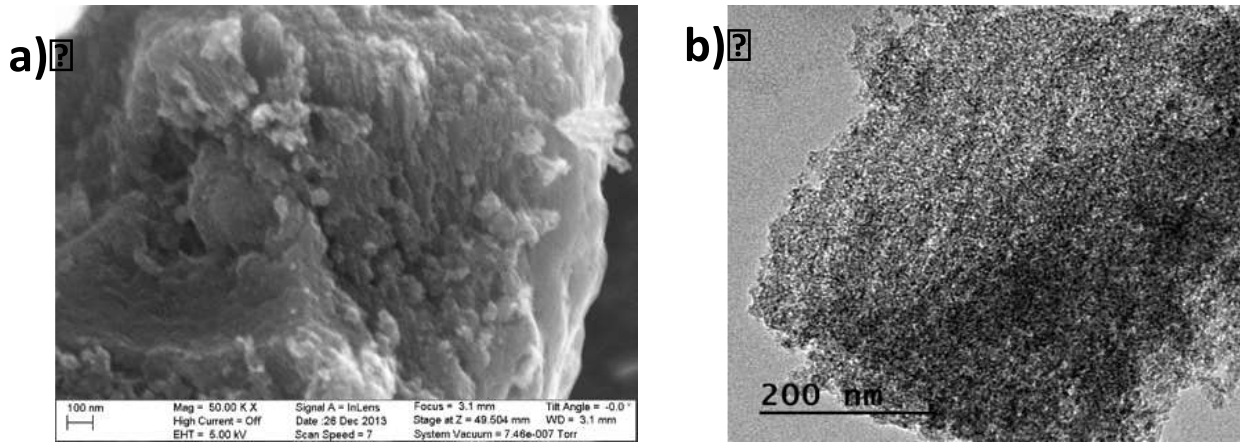

Figure 3. SEM (A) and HR-TEM (B) images of the BAX-TU-800 sample.

To evaluate the acid-base properties of the carbons' surfaces, potentiometric titration experiments were carried out. Table 4 summarizes surface pH and pK_a values for the species present on the carbons' surfaces. All four carbons show similar types of acidic groups but differ in their amounts. On BAX-TU-800 the largest number of acidic groups is detected, especially in the category of strongly acidic groups with the $pK_a<7$. As the XPS analysis indicated, the high amount of strong acidic groups on BAX-TU-800 are assigned to carboxylic acids. These acidic groups were decomposed at high temperature. The low surface pH of BAX-TU-950 are due to the formation of strongly acidic groups, which corresponds to the presence of the N-oxides groups ($pK_a=0.79$).[27] as indicated from the surface XPS results. This species is outside the detection range of the titration technique applied.

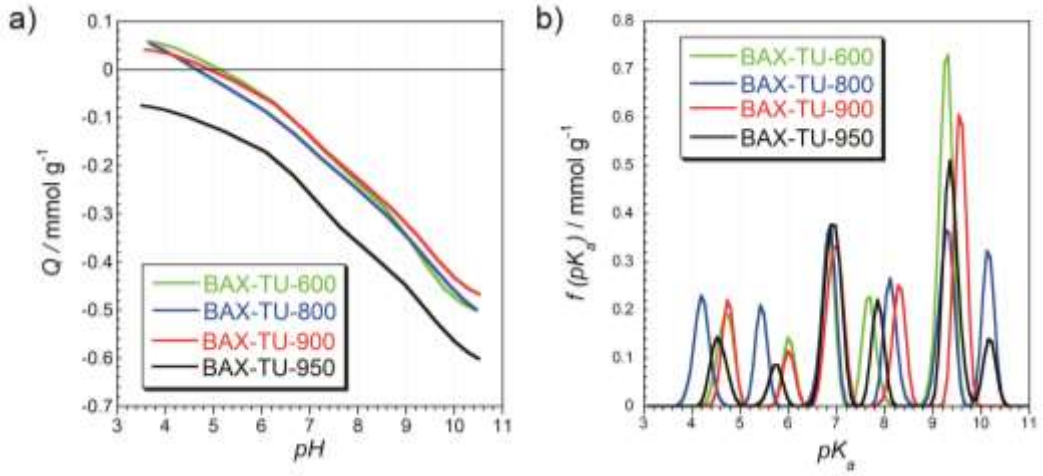

Figure 4. a) Proton binding curves; b) pK_a distributions of the studied samples.

Table 4. Surface pH values, peak positions and numbers of groups (in parentheses, [mmol/g]) for the material studied.

Sample	Surface pH	pK_a 4-5	pK_a 5-6	pK_a 6-7	pK_a 7-8	pK_a 8-9	pK_a 9-10	pK_a 10-11	Strong Acidic Groups (pH<7)	All Groups
BAX-TU-600	4.86	4.69 (0.080)		6.01 (0.044) 6.83 (0.116)	7.68 (0.080)		9.26 (0.262)		0.240	0.582
BAX-TU-800	4.60	4.20 (0.090)	5.44 (0.065)	6.83 (0.133)		8.12 (0.088)	9.27 (0.141)	10.15 (0.103)	0.288	0.619
BAX-TU-900	4.62	4.75 (0.071)		6.01 (0.036) 6.96 (0.145)		8.29 (0.086)	9.57 (0.196)		0.252	0.534
BAX-TU-950	3.75	4.56 (0.059)	5.73 (0.030)	6.92 (0.167)	7.86 (0.070)		9.37 (0.188)	10.17 (0.045)	0.256	0.560

The CO_2 electroreduction was monitored under controlled potentials and the FE for CO_2 reduction were calculated based on the moles of products detected. Figures 5a and 5c show the trends in the FE for CO and CH_4 formation at the 5h reduction process. All potentials reported here are referenced to a reversible hydrogen electrode (RHE). CO was the main reaction product of CO_2EER. The potential at which the specific product was first detected was considered as an onset

potential. As seen in Figure 5a, CO was first detected at -0.37V on BAX-TU-950, which corresponds to the onset overpotential of 0.27V for the CO formation given the equilibrium potential of -0.11V (vs. RHE). This onset potential is lower than those reported for metal electrodes, metal nanostructured, and metal-free electrocatalysts.[1,28,29] For example, the onset potential for copper was reported to be -1V.[28] The onset potential of nanostructured Ag and nitrogen-doped carbon nanotube catalysts were reported as 0.6V and 0.5 V, respectively.[1,29] The low onset overpotential on BAX-TU-950 could be due to its porous structure that favors CO_2 reduction via employing the adsorption forces.[18] The FE for CO formation increased with the potential becoming more negative. It reached the maximum of 29% at -0.67 V at the 5 h reduction process. In comparison to the previous studies,[13,18] BAX-TU-950 showed the highest FE for CO among all nanoporous carbons used as-received, without an additional step of the surface electroreduction.[13,30] In our previous study, one of the samples tested was obtained at a similar treatment procedure as was BAX-TU-950 but it was impregnated with melamine instead of thiourea.[13] The actual atomic concentrations of pyridinic-N, pyrrolic-N, quaternary-N and N-oxides on that carbon were 1.3 at. %, 1.3 at. %, 0.87 at. % and 0.43 at. %, respectively (Figure. 6). Its best FE for the CO formation was 24% at -0.66V at 6h CO_2 reduction. Thus, the sample treated with thiourea overperforms that one treated with melamine. The XPS data of thiourea treated BAX-TU-950 indicates actual atomic concentrations of pyridinic-N, quaternary-N and N-oxides as 0.27 at. %, 0.87 at. % and 0.36 at. %, respectively. The quaternary-N, which was identified previously as catalytically active, is present on the surface in a similar quantity as that on the melamine treated samples. Interestingly, pyridinic-N that is the most active for the CO_2 reduction is present in lesser quantity than that on the surface of the melamine treated sample. This suggests that besides pyridinic-N and quaternary-N there are other active species catalyzing the CO

formation on the surface of BAX-TU-950. This might be related to the activity of the sulfur-containing species. It has been reported previously that thiophenic-S group brought the activity for CO_2 reduction.[18] The thiophenic-S induces slightly positively charge to the neighboring carbon,[31,32] which can stabilize the COOH*/CO_2^{-}·intermediate. Sulfur in such configuration can be present in small pores, similar in size to CO_2 molecules and can increase the strength of the interactions of the intermediates with the carbon surface in these pores.

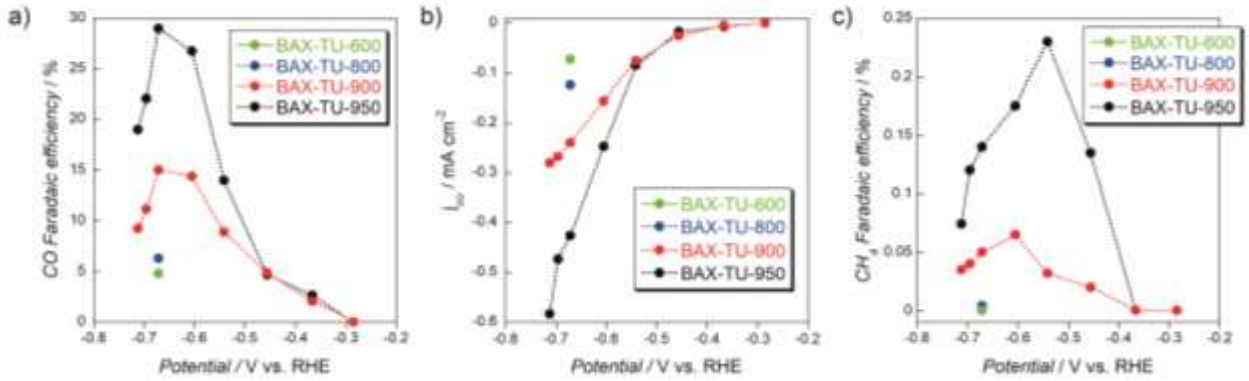

Figure 5. a) Faradaic efficiency for CO formation b) partial current density of CO c) Faradaic efficiency for CH_4 formation at 5h in CO_2-saturated 0.1 M $KHCO_3$

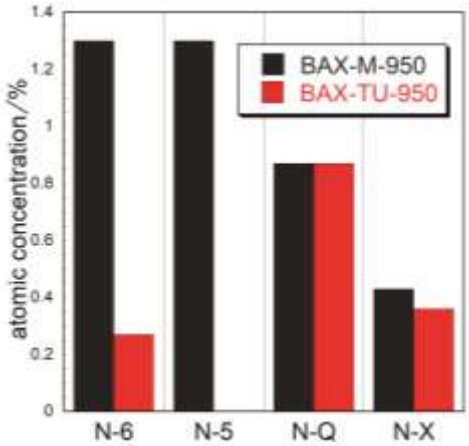

Figure 6. The atomic concentration/distribution of nitrogen species on the surface BAX treated with melamine and thiourea. The data for BAX-M-950 is taken from Ref. [9].

At more negative potentials, the FE of CO formation decreased, which is attributed to higher extent of hydrogen evolution reaction (HER) than that of CO_2ERR.[29,33] The partial CO current densities (j_{co}) as a function of the applied potential were extracted from the data of the controlled potential electrolyses (Figure. 5b). As seen, the kinetics of the reduction process for the CO formation increases linearly as the applied potential becomes more negative than -0.5V. A similar linear relationship for heteroatom doping into carbon materials has been reported in the reduction of CO[1,2,6] and formate[8]. The FEs for CO decreased dramatically for the samples treated at low temperatures. They are 15.0%, 6.3% and 4.8%, BAX-TU-900, 800 and 600, respectively, at 5h reduction at the potential of -0.67V, which is the potential of the maximum FE for CO on BAX-TU-950.

Even though the lower temperature of the heat treatment preserved more heteroatoms (both nitrogen and sulfur) in the carbon matrix, the conductivity of BAX-TU-600 and 800 samples is low, which likely hinders the reduction process involving the electron transfer to the electrode surface. Thus, in spite of the favorable surface chemistry of these samples, their performance might be greatly limited by the low electric conductivity. The results suggest that the most developed porous structure of BAX-TU-600 cannot compensate the limitation of conductivity. These results also suggest that CO_2ERR is not directly related to the porosity.

CH_4 was formed on BAX-TU-950 with the maximum FE of 0.23% at 0.54V, which corresponds to the overpotential of 0.37V. The change in the efficiency with the potential is very similar to that for the CO formation. The FE of BAX-TU-950 for CH_4 formation is the highest among all tested samples. Besides, its overpotential is lower than that of BAX-TU-900. In comparison to our previous results,[13] the samples addressed here are less favorable for the CH_4 formation than were the samples of BAX modified with melamine. The highest FE of CH_4 for the melamine-modified

sample was reported as 0.76% at 6h at -0.66V. Since both melamine and thiourea treated samples showed similar amount of quaternary-N and N-oxides, the lower FE for the methane formation could due to the smaller amount of pyridinic-N on BAX-TU-950. Thus, CO is less likely to be stabilized and further reduced to CH_4 without pyridinic-N. It also infers that thiophenic-S is not as active as is pyridinic-N in the stabilizing CO* intermediate and thus less CH_4 is formed. Since the FE for CH_4 is smaller on BAX-TU-950 than that on BAX-M-950, in spite of the higher volume of micropores in the former sample, more pyridinic-N located in micropores might compensate the enhancing pore size/volume effect on methane formation in the case of BAX-M-950.

Another important feature of an ideal CO_2 reduction electrocatalyst is its stability, given the fact that many polycrystalline metals[34] deactivate in the minute timescale in this catalytic process. We have tested the long-term durability of our carbon catalyst at a constant applied electrode potential of −0.67 V (Fig .5). The best stability was found for BAX-TU-950 with a current density remained steady at -1.5mAcm^{-2} throughout the 40h period (Figure S3). However, the FEs of CO formation first increased and then decreased with the progress of the reduction time. As seen in Figure 8a, the FE of CO for BAX-TU-950 increased from 23% (1h) to 29% (5h) within the first 5h, and then gradually decreased during the reduction process. The sample was detached from the current collector after 40h reduction, which ceased its catalytic performance. On the other hand, the FE of CH_4 for BAX-TU-950 reached its maximum after 24h and then gradually decreased. The stability dramatically decreased for BAX-TU-600, 800 and 900. They lasted for about 18h, 23.8h and 21h, respectively. Figure 8d shows the LSV curves of our catalysts in N_2-saturated $KHCO_3$ electrolyte, at the potential of -0.67V. The higher current density of BAX-TU-600, 800 and 900 indicates the higher HER activity than that of BAX-TU-950. The results indicate that when the catalyst is more favorable to HER, its stability for CO_2 reduction decreases. The detachment of the catalyst film

from the current collector was observed, which could be due to the mechanical strain and stress created from the rapid release of H_2 product from HER.

After CO_2 reduction, a marked decrease in the content of sulfur is found for all samples, likely as a result of surface oxidation during CO_2 reduction (Table 1). As indicated previously, sulfur species incorporated to the carbon matrix are much less stable than are nitrogen ones [13, 18, 35, 36]. Using the catalyst in CO_2ERR caused a slight reduction of the surface of all samples but BAX-TU-600, for which the content of oxygen increased. The small change in the content of nitrogen indicate the stability of this element in the carbon matrix.

The deconvolution of C 1s core energy level spectra of the used catalysts confirms the general trend in surface reduction. A detailed look at N 1*s* core energy level spectra shows that while the contribution of pyridines decreased for BAX-TU-600 and BAX-TU-800, their amounts are very stable for BAX-TU-900 and BAX-TU-950. Since these species were indicated before as most catalytically active for CO_2 reduction[13,14,18] these XPS results, combined with the good performance of these samples, support the mechanism proposed previously on the important role of positively charged centers in stabilization of COOH*/ $CO_2^{-}\cdot$ intermediates in CO_2 electroreduction.[13, 18] On the other hand, sulfur in the best performing showed the highest level of oxidation and the reduced sulfur species, besides providing centers for CO_2 reduction [13] might also protect nitrogen catalytic sites by undergoing oxidation reactions.

Since we hypothesized that the adsorptive interactions are important for CO_2 electroreduction, CO_2 adsorption isotherms at 20 ^{o}C were measured up to atmospheric pressure and they are presented in Figure 7. Even though BAX-TU-600, which has the smallest volume of micropores, revealed the smallest quantity of CO_2 adsorbed, the lack of a direct relationship between the amount adsorbed and the volume of small pores indicates the importance of N- and S- rich surface for

CO_2 specific interaction/reactions with carbon.[35,36] The volume of small pores in all samples but that modified at 600 ºC are similar and the slightly higher amount of CO_2 adsorbed on BAX-TU - 800 might be related to its high content of sulfoxide and sulfones which might attract CO_2 in a specific way.[37]

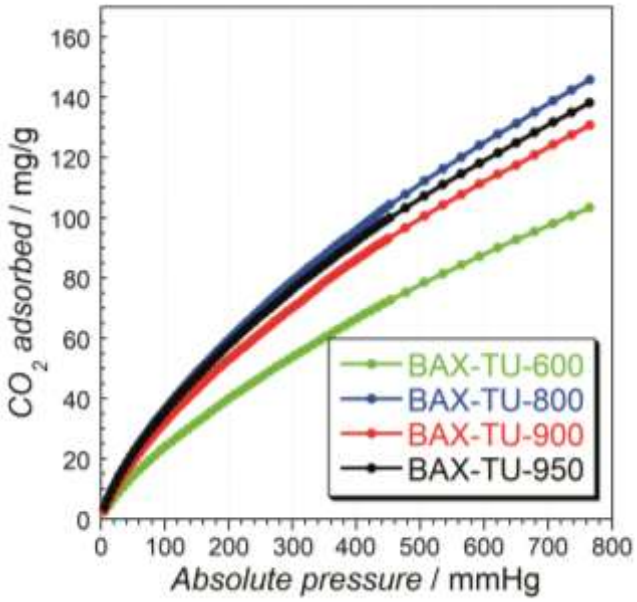

Figure 7. CO_2 adsorption isotherms at 20 ºC.

The surface pH is also expected to have an effect of CO_2 electroreduction with acidic surface increasing Faradaic efficiency for H_2 and CH_4 formation. It is seen in Figure 6c, surface acidity might enhance formation of CH_4 on BAX-950 compared to that on BAX-900. Their porosities are quite similar, but the pH of the former samples is much lower that of the latter one.

To exclude that the decomposition of the carbon catalysts themselves is responsible for the formation of CO or CH_4, the reduction experiments were carried out in N_2 saturated electrolyte at -0.67 V vs. RHE. No CO and CH_4 were detected for all the BAX-TU materials through the whole reduction process.

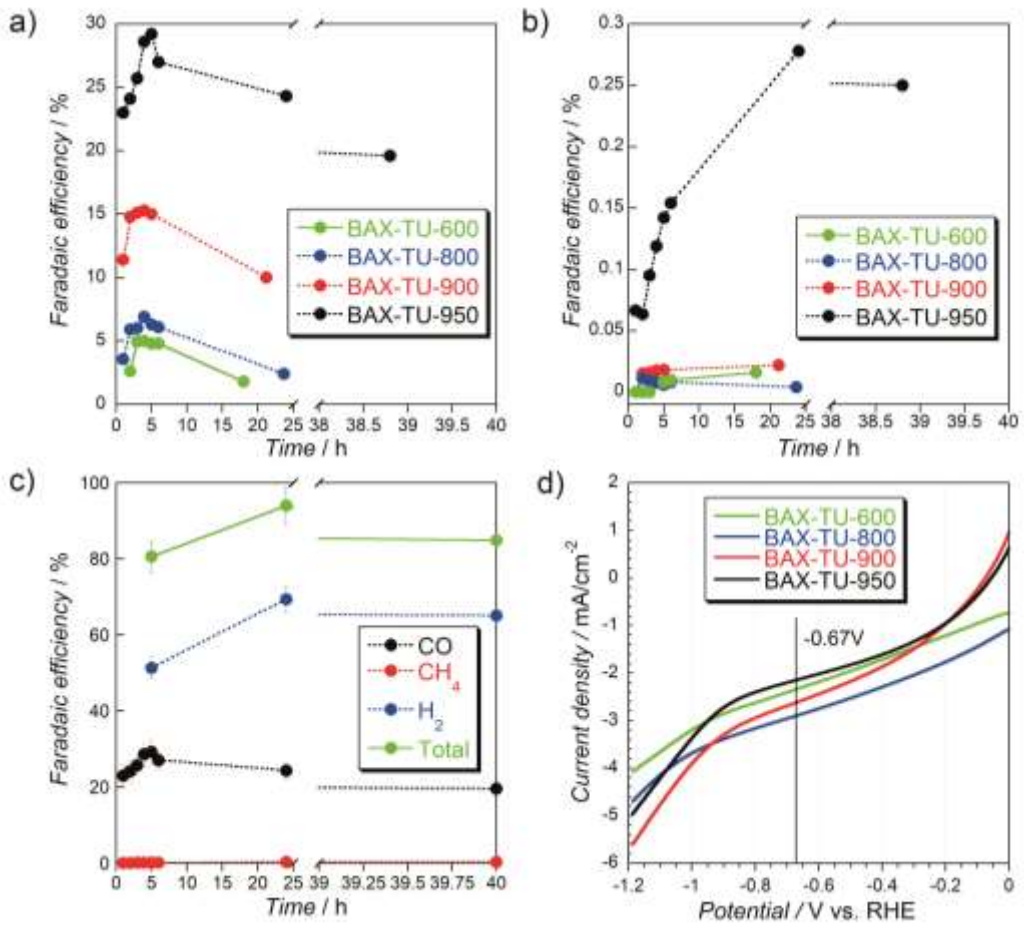

Figure 8. a) Faradaic efficiency for CO formation; b) Faradaic efficiency for CH_4 formation during CO_2 reduction at the potential -0.67 V vs. RHE; c) The FE for detected gas phase of BAX-TU-950 for 40h; d) LSV for the materials studied in N_2 saturated 0.1M $KHCO_3$

The total FE was accounted for 80%-90% throughout the reduction process on the BAX-TU-950 catalyst (Figure 8c). The capacitive charging behavior of carbons, the adsorption of the produces in pores and the presence of dissolved products in the electrolyte can contribute to missing 10-20 %. In addition, the leakage of H_2 gas after 24h reduction could take place due to the imperfect sealing of the electrochemical cell. To verify whether or not liquid products were formed, NMR

analysis of the electrolytes after CO_2 reduction was carried out. The ^1H NMR spectra are presented in Figure S4 of the Supporting Information. Trace amounts of C_1 products (methanol, formic acid) and C_3 products (acetone) were detected in the electrolytes of all the samples. Their quantification is beyond the scope of this paper.

To test the effect of light on the CO_2 electroreduction, BAX-TU-950 and BAX-TU-600 were chosen since they showed the lowest and highest content of sulfur among four samples studied. Their photosenistivities were first tested. The repeatable transient photocurrents upon on/off irradiation are shown in Figure 9. As seen, the photocurrent increased upon light irradiation on both materials. The photocurrent generated (based on the initial current) was 3.3% and 46.8% for BAX-TU-950 and BAX-TU-600, respectively. Even though the initial current of BAX-TU-600 (0.44mA) is 2 order magnitude less than that of BAX-TU-950 (43mA), the percentage of the generated photocurrent showed that BAX-TU-600 was much more photoactive than was BAX-TU-950.

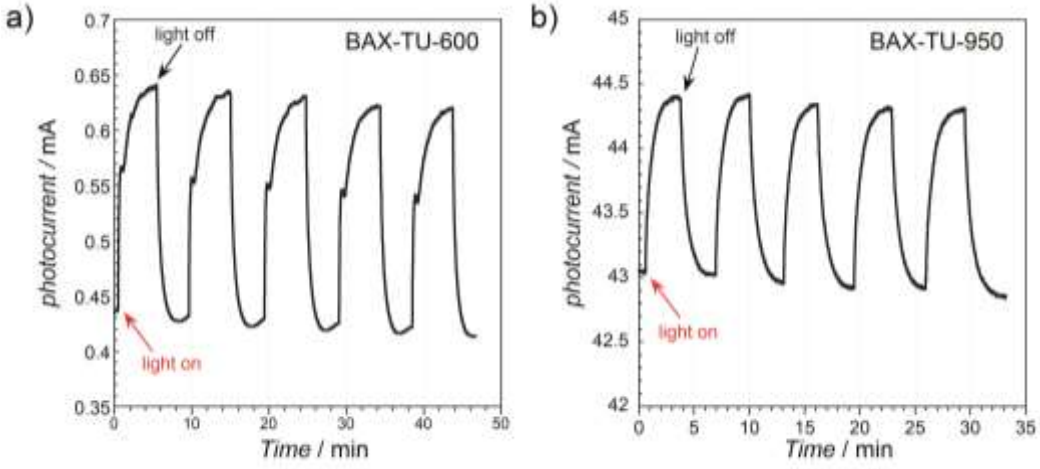

Figure 9. Photocurrent generation upon on/off visible light radiation at voltage 1 V on a) BAX-TU-600 and b) BAX-TU-950.

To find out how light affects the CO_2 reduction, the reduction process was first performed in the dark conditions for 4h at the potential of -0.67V. Then the electrode was exposed to solar light (150 W Xe lamp). Upon irradiation, the absolute value of the current density for both samples increased and remained stable at the higher current density (Figure 10a) than those under dark. The FE for the CO formation at 5h was 27.0% and 4.4% for BAX-TU-950 and BAX-TU-600, respectively. When the CO_2 reduction was conducted in the dark for 5h, the FE for CO on BAX-TU-950 and BAX-TU-600 was 29.0% and 4.8%, respectively. Thus, the FE of CO slightly decreased under irradiation for both materials. While the partial CO current density of BAX-TU-950 increased 21%, for BAX-TU-600 that increase was 28%, in comparison to those measured in the dark (Figure 10b). The formation rate of CO on BAX-TU-950 and BAX-TU-600 under irradiation were 15.8 μmol/h and 3.9 μmol/h, respectively. The formation rate under irradiation are higher than those under dark (Table S1). These results are very promising in comparison with those reported in the literature. Thus on plasmonic Au/p-GaN the rate of CO formation was 5 nmol/h for CO formation.[38] On CoII(Ch)-modified cathode the highest rate measured was 0.58 μmol/h at pH of 6.7[39] and on Ag-loaded boron-doped diamond (BDD) electrodes the reported rate with 5.97μmol/h.[40]

Assuming that the rest of the current is used for HER, the partial H_2 current density of BAX-TU-950 and BAX-TU-600 increased 28% and 41%, respectively, in comparison to those in the dark. The results suggest that the generated photoelectrons contributed to both CO_2 and HER reduction. The photoinduced electrons were accepted by both CO_2 and water and more of them was used for HER than that for CO_2 reduction. Based on XPS analysis, more thiophenic-S was present on the BAX-TU-600 surface, and this configuration seems to enhance the generation of photocurrent along with an increase in the current linked to the CO formation.

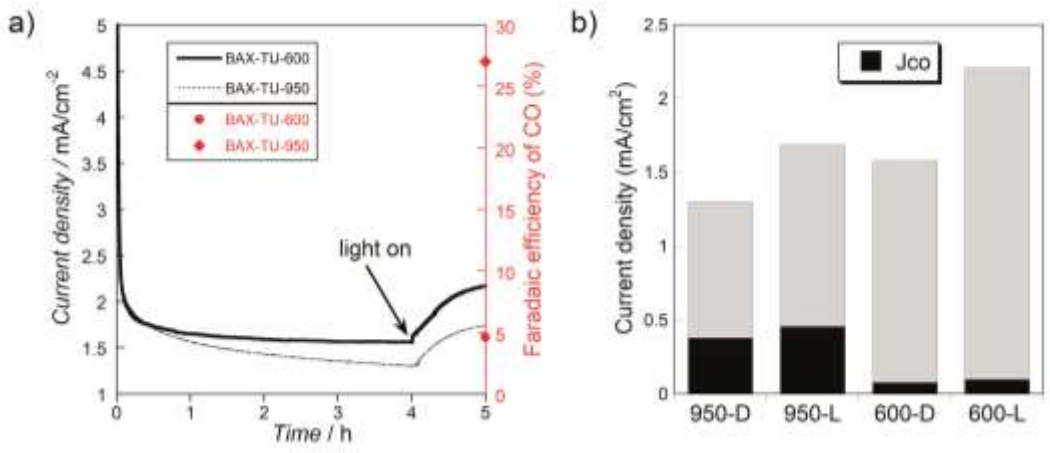

Figure 10. a) The current density and FE of CO upon light for BAX-TU-600 and BAX-TU-950; b) Comparison of the total current density and CO partial current density measured in the dark and at light for both BAX-TU-950 and BAX-TU-600.

Tafel analyses (Figure 11) have been performed to elucidate the kinetics associated with the reduction of CO_2 to CO. The obtained Tafel slope is 153 mV dec^{-1} and 146mV dec^{-1} for the BAX-TU-900 and BAX-TU-950, respectively. Those values are close to 118 mV dec^{-1}, which is expected for a rate-limiting single-electron transfer at an electrode.[41] For nitrogen-doped carbon nanotube(NCNT) the Tafel slope was reported to be 203 mV/dec.[1] Another study reported the lowest value of 160 mV dec^{-1} among the NCNTs.[2] This suggests the nanoporous carbons present fast kinetics for CO formation and faster than those on CNT. This could be due to the porous structure of the carbon. Even though the developed pore structure is not a necessary factor governing the catalytic activity for the CO formation, it seems beneficial for the overall reduction process. The previous studies indicated that the positively charged sites, especially the positively charged carbon atoms introduced from pyridinic-N and quanternary-N are the active sites for CO formation.[13,18] The thiophenic-S also introduces the positive charge to the carbon atoms although it is less electronegative than nitrogen is, which results in a lower the activity for the CO formation

than that brought by pyridinic-N. The introduction of sulfur, on the other hand, also lowers the conductivity of the carbon. Since the electric conductivity of plays a crucial role for CO_2 reduction, increasing simultaneously the positively charged sites as well as conductivity would be the future goal to achieve a high efficiency of CO_2 reduction.

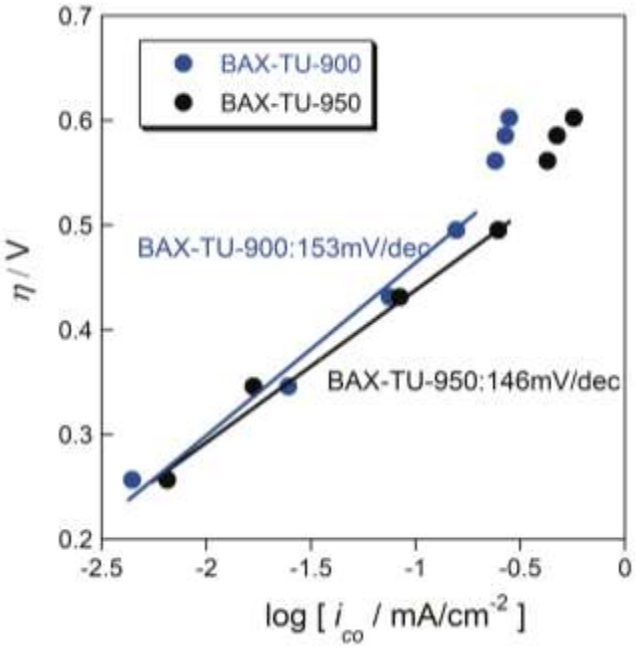

Figure 11. Tafel plots for BAX-TU-900 and BAX-TU-950.

To check if exposure to light affect the electron transfer on the samples tested, the impedance spectra of BAX-TU-950 and BAX-TU-600 were measured in the $KHCO_3$ electrolyte saturated with CO_2 (Figure 5S of the Supplementary Information). While for BAX-YU-950 exposure to light resulted in a visible decrease the high frequency arch indicating an increase in charge transfer[42], the results for BAX-TU-600 do show any effect of light on electron transfer. This might be caused by limitation of the conductivity of the carbon and also in its chemical instability, as shown in the XPS data.

To date, this is the first report on the solar light influence on the CO_2 electroreduction on carbonaceous catalysts. The results suggest that upon light, thiophenic-S increases carbon photsensitivity and promotes the CO formation. To further understand the nature of the process, the band gaps and band alignments were estimated from the Mott-Schottky plots (Figure S6 of the Supporting Information) from electrochemical impedance spectroscopy (EIS) measurements (Figure 12a). The photoactive catalyst should have a band gap of less than 3.18eV in order to adsorb visible light. BAX-TU-600 and BAX-TU-950 shows band gap of 1.91eV and 3.02eV, respectively. The smaller bandgap of BAX-TU-600 in comparison to that of BAX-TU-950 might explain its higher photoactivity. Moreover, the position of the conduction band (CB) of BAX-TU-600 is more favorable than that of BAX-TU-950 for both the CO_2 reduction and H_2 evolution reaction, which is consistent with the higher extent of photocurrent generation at light on BAX-TU-600 as compared to that on BAX-TU-950.

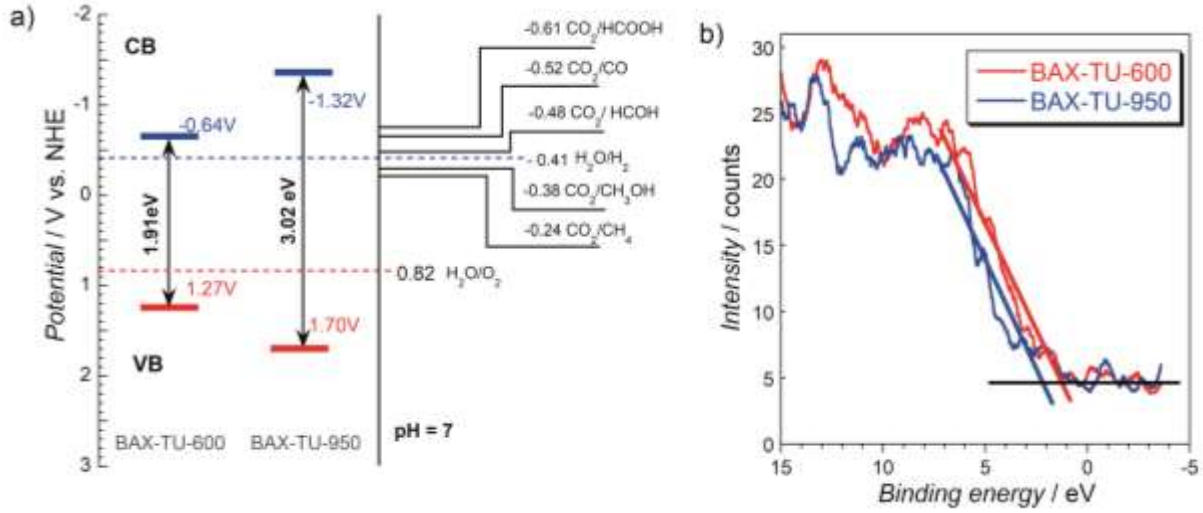

Figure 12. a) Band-gap diagram of BAX-TU-600 and BAX-TU-950 (The CO_2 redution reactions must involve protons from water); b)XPS valence spectra of BAX-TU-950 and BAX-TU-600.

To further confirm the difference in the bandgap, the XPS valence spectra for BAX-TU-600 and BAX-TU-950 were collected[43]. The results are presented in Figure 12b. Since in the case of carbon the valence and conduction bands are rather the apparent values related to local electronic structures[44] [49], we consider these results as a rather semiquanitative than quantitative estimation of the valence band position. Nevertheless, the results indicated that the valance band of BAX-TU-950 is at higher energy than that of BAX-TU-600 and this trend is in agreement with our estimation illustrated in Figure12a.

Conclusions

From all three N and S-co-doped carbon addressed in this research, the sample modified at 950 ^{o}C showed the highest activity at a low overpotential for CO formation in the process of CO_2ERR. This sample also showed the longest stability. Besides pyridinic-N, the catalytic activity of thiophenic-S was found to contribute to its high FE for the CO formation. The results were better than those obtained on the previously studied nitrogen-doped carbon. However, the activity of that carbon for the CH_4 formation was smaller than that of pyridinic-N. The increase in the performance with the increase in the heat treatment temperature indicates the importance of an electric conductivity for the CO_2ERR process.

In this first study of sulfur modified carbons as CO_2 (photo)electrocatalysts for CO_2ERR. Thiophenic-S was found to play a crucial role in generating photocurrent upon light, which is beneficial for the overall reduction process (both hydrogen evolution reaction and CO_2 reduction). Thus, the obtained results advance the development of state-of-art metal-free catalyst for the CO_2 reduction through engaging the catalytic activity and photoactivity provided by the incorporation

of sulfur to the carbon matrix. The findings have significant implications for the understanding of the CO_2 reduction process and functional sulfur-carbon moieties.

Experimental Section

Materials

A wood-based commercial activated carbon BAX-1500 (Mead Westvaco), which is referred to as BAX was chosen for this study. The BAX was soaked in a thiourea suspension (mass ratio=1:1) in water for 24h under stirring at a room temperature. The mixture was then heated to evaporate water and dried at 120 ^{o}C. As the next step, the samples were heated to 600, 800, 900 and 950 ^{o}C with rate of 20 ^{o}C/min (under N_2). The final temperature was kept for 30 min. After carbonization, the samples were washed with deionized (DI) water at 80 ^{o}C for 4h in a 2-liter beaker to remove the excess of the thiourea and water-soluble compounds. Then they were filtered and washed with DI water until the pH of leachate was 7. The samples were dried at 120 ^{o}C overnight. Following the treatment, the samples are referred to as BAX-TU-600, BAX-TU-800, BAX-TU-900, BAX-TU-950, where last three digits refer to the heating temperature.

X-ray Photoelectron Spectroscopy (XPS)

The XPS spectra were collected using the Physical Electronics PHI 5000 VersaProbe II spectrometer with a monochromatic Al Kα (1486. 6 eV) radiation operating at 15 kV and 50 W in the analyzer chamber. Prior to analysis, all samples were outgassed until 10^{-8} Torr at room temperature. High-resolution spectra of samples were collected with the constant pass energy values of 29.35 eV and a 200 μm diameter analysis area with a take-off angle of 45^{o}. 117.4 eV pass energy was used for the survey spectra and the calculation of surface atomic concentration. The spectrometer energy scale was calibrated using Cu $2p_{3/2}$, Ag $3d_{5/2}$, and Au $4f_{7/2}$ photoelectron

lines at 932.7, 368.3, and 84.0 eV, respectively. The SmartSoft-VP2.6.3.4 software package was used for acquisition and data analysis and Multipack software was used to fit deconvoluted photoelectron spectra. A Shirley-type background was subtracted from the signals and recorded spectra were fitted using Gauss–Lorentz method in order to determine the binding energy of the different element core levels accurately. XPS valence spectra was collected with 11.75 eV pass energy at which the instrumental resolution is about 0.05 eV.

Sorption of nitrogen/porosity evaluation

Sorption of nitrogen was measured on ASAP 2020 Surface Area and Porosity Analyzer (Micromeritics) at -196 ^{o}C. Before analysis, the samples were outgassed at 120°C to constant vacuum (10^{-4} Torr). At these conditions only physically adsorbed species were removed without changing the surface chemistry. The surface areas (NLDFT method), total pore volumes (V_t), the volumes of mesopore (V_{meso}), micropore (V_{mic}), ultramicropore ($V_{<0.7nm}$) and the volume of pores smaller than 1 nm ($V_{<1\ nm}$), were calculated from the isotherms using the Non-Linear Density Functional Theory (NLDFT) www.nldft.com.[45,46] The pore size distributions were also calculated using this method.

Adsorption of CO_2

Adsorption of CO_2 was measured at 20 ^{o}C until 760 torr on ASAP 2020. Before analysis, the samples were outgassed at 120°C to constant vacuum (10^{-4} Torr). The temperature was controlled using a circulating water bath.

SEM and TEM Electron microscopy

SEM images were obtained with a Zeiss Supra 55 VP at a magnification 100 KX with an accelerating voltage of 5.00 kV. Scanning was performed in situ on a sample of powder without

coating. HR-TEM was performed using a JEOL 2100 LaB6 instrument operating at 200 kV. Analyses were performed after the carbon samples were resuspended in isopropyl alcohol.

DC Conductivity measurements

A film of a sample dispersed N-methyl-2-pyrrolidone (NMP) was coated on a 0.5 cm × 0.45 cm gold interdigitated electrode. The samples were dried at 120 °C for 24 h to evaporate the NMP solvent. The sheet resistance was measured with a 4-probe method using Keithley 2400 Multimeter. Then the DC conductivity was calculated in the following formula:

$$\sigma = \frac{1}{R} \cdot \frac{L}{W \cdot t}$$

where L is the length of the electrode, W is the wideness of the electrode, t is the thickness of the electrode, σ is the conductivity of the material and R is the measured sheet resistance. The sample film's thickness was measured by a digital micrometer (Pittsburgh®). Each material was tested three times and the average values were reported.

Potentiometric titration

Potentiometric titration analysis was carried out on the DMS Titrando 888 automatic titrator (Metrohm). The samples (~ 0.050 g) were added to 25 mL of $NaNO_3$ (0.01 M), and equilibrated overnight at a room temperature. The suspension was saturated with N_2 throughout the measurements under a continuous stirring to eliminate the influence of atmospheric CO_2. Each sample was titrated with volumetric standard NaOH (0.1 M) after adding 0.1M HCl to the sample suspension. The initial pH of the suspension was used as the surface pH value. The experimental data were transformed into proton binding curves, Q, and then to pK_a distributions. The pK_a distributions were calculated using SAIEUS numerical procedure [45,47].

CO_2 electrochemical reduction measurement

To prepare a working electrode, a homogeneous slurry of an active material with polyvinylidene fluoride (PVDF) and carbon black (mass ratio 8:1:1) in N-methyl-2-pyrrolidone (NMP) was first prepared. A uniform 5 ± 0.2mg/cm^2 catalyst was coated double sides on to a Titanium (Ti) foil (1 cm^2). Such prepared electrodes were dried at 100^{o}C overnight in an oven. Since the Ti foil was fully covered by a layer of the catalyst, it was assumed that the current generated on Ti did not affect our results in a marked way.

The CO_2ERR was evaluated at different reduction potentials in CO_2 (ultrapure 99.99%) saturated $KHCO_3$ electrolyte (0.1 M) on VersaSTAT MC (AMETEK, Princeton Applied Research). The tests were performed in an airtight three-electrode and two compartments cell separated by a cation exchange membrane (Nafion 117). Ag/AgCl/NaCl (3M) was used as a reference electrode and Pt wire as a counter electrode. The resistance of the electrochemical cell was measured before the CO_2ERR experiments using an IR compensation. A measured cell resistance was approximately 45 Ω for all the catalyst samples. After the testing, the data were corrected for the cell resistance. Before the electrochemical CO_2 reduction reaction, the electrodes were wetted in $KHCO_3$ (0.1 M) for 4 h with an open circuit potential (OCP) vs. Ag/AgCl was recorded. Then the cyclic voltammetry (CV) experiments were run in the potential window from 0 V to -1.5 V vs. Ag/AgCl to test the stability with an increase in the number of cycles. The OCP and CV measurements were performed in a N_2-saturated electrolyte. Potential values are reported versus reversible hydrogen electrode (RHE): E (vs. RHE) = E (vs. Ag/AgCl) + 0.21 V + 0.059×pH (pH of saturated CO_2 0.1M $KHCO_3$ is 6.8). Before CO_2ERR, the electrolyte was purged with CO_2 for 30 min and headspace of the cell for 20 min. Then the chronoamperometry (CA) was run under constant potentials between -0.3 V and -1.2 V vs. RHE for 6h at ambient light. The Tafel plot was derived following Equation (1):

$$E - E_0 = \eta = a + b \log j_{co} \quad (1)$$

where E is the applied potential, E_0 is the equilibrium potential (−0.11V vs RHE for the CO_2/CO) in a pH 7.0 aqueous solution, η is the overpotential for CO_2/CO, b is the Tafel slope and j_{co} is partial current density for CO formation at various potentials.

During the CA run, the gas phase products from the headspace of the cathodic compartment of the electrochemical cell were analyzed every hour using gas chromatograph (GC) (model SRI 8610C). The gas phase was injected into the GC column with a gastight syringe and the separation was done on a Carboxen column (Carboxen-1000, 4.57 m in length, and 2.1 mm in internal diameter). The GC oven heating program was as follows: 35 ^oC for 5 min, then heating from 35 to 220 ^oC at a rate of 20 ^oC/min and holding at 220 ^oC for 5 min. The carrier gas was He with a flow rate of 30 mL/min. A flame ionization detector (FID) was used to detect hydrocarbons, and a thermal conductivity detector (TCD) was used to detect CO and H_2. CO and CH_4 were the target reduction products. Even though the concentration of CH_4 was very small, it was in the range of the amount used to calibrate the detector (R^2=0.992). Additionally, the content of the electrolyte solution after 48h CO_2ERR was tested using NMR. ^{1}H NMR data were acquired at 298 K on a Bruker 800 MHz Advance III HD spectrometer equipped with a 5-mm TCI cryoprobe. 1D ^{1}H NMR spectra were recorded with a sweep of 16 ppm centered on the water, 1.7 s acquisition time, 2 s relaxation delay, gradient excitation sculpting water suppression, for the total of 512 scans.

To study the influence of light on the CO_2 reduction on our samples, the reduction process was carried in the cell isolated from light exposure for 4h. At 4h, the 150W Xe lamp (Solar Light Co., INC, XPS-150™) was used as the irradiation source. The light shined on one face of electrode. A mirror was set facing a counter electrode cell in such a way that the solar light could reflect to the

other side of working electrode. The FE of CO was monitored every 1h using GC as described above.

Photoelectrochemical measurements

The experimental setup used is illustrated in the literature.[48] Basically, a slurry of the sample and N-methyl-2-pyrrolidone was coated on a 0.5 cm × 0.45 cm thin-film gold interdigitated electrode. The samples were dried at 120 °C for 24 h with the film thickness of ~100 μm. The 150 W Xe lamp (Solar Light Co., INC, XPS-150™) was used as an irradiation source and a pyrex filter (cut-off below 420 nm) was used to select visible light. The electrical measurements were carried out using a VersaSTAT MC (AMETEK, Princeton Applied Research) through four-wires at room temperature. The photocurrent was tested through chronoamperometry at 1V and it was repeated five times with and without radiation.

Electrochemical Impedance Spectroscopy (EIS)

EIS was performed at -0.67 V RHE in the CO_2 saturated 0.1M $KHCO_3$ electrolyte with an AC voltage amplitude of 5 mV and a frequency range from 10 kHz to 0.01 Hz with or without irradiation (150 W Xe lamp).

Band gap estimation

The impedance spectroscopy was carried out in 0.5 M Na_2SO_4, in a three-electrode cell, using Ag/AgCl (3 M NaCl) as a reference electrode, the active material- as a working electrode, and a platinum rod- as a counter electrode. The working electrode was prepared the same way as mentioned in the CO_2 elctroreduction experiment description. Potentiostatic electrochemical impedance spectroscopy (EIS) measurements were performed using VersaSTAT MC (AMETEK, Princeton Applied Research) in the frequency range of 0.05 Hz–100 kHz with a 10 mV AC

amplitude, at various potential vs. reference electrode, ranging from −0.9 V to 0.90 V (0.69 V–1.11 V vs. NHE). The initial pH of 0.5 M Na_2SO_4 was 6.43. From the results Mott-Schottky plots were constructed[49] and band gap positions were calculated[49].

Acknowledgements

This research was partially funded by NSF CBET Grant No. 1133112. The authors would like to acknowledge the Surface Science and Biomolecular NMR Facility of CUNY Advanced Science Research Center for instrument use and technical assistance. The experimental help of Dr. Marc Florent is appreciated.

Conflicts of interest

There are no conflicts to declare.

Keywords: CO_2 photoelectrochemical reduction, porosity, thiophenic sulfur, photoactivity, CO and CH_4 Faradaic efficiency.

References

[1] J. Wu, R. M. Yadav, M. Liu, P. P. Sharma, C. S. Tiwary, L. Ma, X. Zou, X.-D. Zhou, B. I. Yakobson, J. Lou, et al., *ACS Nano* **2015**, *9*, 5364–5371.

[2] P. P. Sharma, J. Wu, R. M. Yadav, M. Liu, C. J. Wright, C. S. Tiwary, B. I. Yakobson, J. Lou, P. M. Ajayan, X. D. Zhou, *Angew. Chemie - Int. Ed.* **2015**, *54*, 13701–13705.

[3] J. Xu, Y. Kan, R. Huang, B. Zhang, B. Wang, K.-H. Wu, Y. Lin, X. Sun, Q. Li, G. Centi, et al., *ChemSusChem* **2016**, *9*, 1085–1089.

[4] J. Melorose, R. Perroy, S. Careas, Y. Zheng, Y. Jiao, L. H. Li, T. Xing, Y. Chen, M.

Jaroniec, S. Z. Qiao, et al., *ACS Nano* **2014**, *5*, 1–8.

[5] W. Zhang, Y. Hu, L. Ma, G. Zhu, Y. Wang, X. Xue, R. Chen, S. Yang, Z. Jin, *Adv. Sci.* **2018**, *5*, DOI 10.1002/advs.201700275.

[6] B. Kumar, M. Asadi, D. Pisasale, S. Sinha-Ray, B. a Rosen, R. Haasch, J. Abiade, A. L. Yarin, A. Salehi-Khojin, *Nat. Commun.* **2013**, *4*, 2819–2826.

[7] M. Li, T. Liu, X. Bo, M. Zhou, L. Guo, S. Guo, *Nano Energy* **2017**, *33*, 221–228.

[8] H. Wang, Y. Chen, X. Hou, C. Ma, T. Tan, *Green Chem.* **2016**, *18*, 3169–3458.

[9] J. Wu, S. Ma, J. Sun, J. I. Gold, C. Tiwary, B. Kim, L. Zhu, N. Chopra, I. N. Odeh, R. Vajtai, et al., *Nat. Commun.* **2016**, *7*, 13869.

[10] G. Zhu, L. Ma, H. Lv, Y. Hu, T. Chen, R. Chen, J. Liang, X. Wang, Y. Wang, C. Yan, et al., *Nanoscale* **2017**, *9*, 1237–1243.

[11] Y. Song, W. Chen, C. Zhao, S. Li, W. Wei, Y. Sun, *Angew. Chemie Int. Ed.* **2017**, *56*, 10840–10844.

[12] H. Wang, J. Jia, P. Song, Q. Wang, D. Li, S. Min, C. Qian, L. Wang, Y. F. Li, C. Ma, et al., *Angew. Chemie - Int. Ed.* **2017**, *56*, 7847–7852.

[13] W. Li, B. Herkt, M. Seredych, T. J. Bandosz, *Appl. Catal. B Environ.* **2017**, *207*, 195–206.

[14] W. Li, N. Fechler, T. J. Bandosz, *Appl. Catal. B Environ.* **2018**, *234*, 1–9.

[15] M. Nakazawa, Y. Mizobe, Y. Matsumoto, Y. Uchida, M. Tezuka, M. Hidai, *Bull. Chem. Soc. Jpn* **1986**, *59*, 809–814.

[16] Y. Kushi, H. Nagao, T. Nishioka, K. Isobe, K. Tanaka, *Chem. Lett.* **1994**, 2175–2178.

[17] B. Dembinska, W. Kiciński, A. Januszewska, A. Dobrzeniecka, P. J. Kulesza, *J. Electrochem. Soc.* **2017**, *164*, H484–H490.

[18] W. Li, M. Seredych, E. Rodríguez-Castellón, T. J. Bandosz, *ChemSusChem* **2016**, *9*, 606–616.

[19] K. Singh, M. Seredych, E. Rodriguez Castellon, T. J. Bandosz, *ChemElectroChem* **2014**, *1*, 565–572.

[20] T. J. Bandosz, J. Matos, M. Seredych, M. S. Z. Islam, R. Alfano, *Appl. Catal. A Gen.* **2012**, *445–446*, 159–165.

[21] M. Seredych, T. J. Bandosz, *Fuel* **2013**, *108*, 846–849.

[22] M. Seredych, L. Messali, T. J. Bandosz, *Carbon* **2013**, *62*, 356–364.

[23] M. Seredych, T. J. Bandosz, *Appl. Catal. B Environ.* **2014**, *147*, 842–850.

[24] C. O. Ania, M. Seredych, R.-C. Enrique, T. J. Bandosz, *Carbon* **2014**, *79*, 432–441.

[25] S. R. Kelemen, M. L. Gorbaty, P. J. Kwiatek, *Energy & Fuels* **1994**, *8*, 896–906.

[26] S. Glenis, A. J. Nelson, M. M. Labes, *J. Appl. Phys.* **1999**, *86*, 4464–4466.

[27] D. Lide, *CRC Handbook of Chemistry and Physics, Internet Version 2005*, <http://www.hbcpnetbase.com>, CRC Press, Boca Raton, FL, **2005**.

[28] K. P. Kuhl, E. R. Cave, D. N. Abram, T. F. Jaramillo, E. Environ, *Energy Environ. Sci.* **2012**, *5*, 7050–7059.

[29] Q. Lu, J. Rosen, Y. Zhou, G. S. Hutchings, Y. C. Kimmel, J. G. Chen, F. Jiao, *Nat. Commun.* **2014**, *5*, 3242–3247.

[30] W. Li, Y. Hu, E. Rodríguez-Castellón, T. J. Bandosz, *J. Mater. Chem. A* **2017**, *5*, 16315–16325.

[31] Z. Yang, Z. Yao, G. Li, G. Fang, H. Nie, Z. Liu, X. Zhou, X. X. Chen, S. Huang, *ACS Nano* **2012**, *6*, 205–211.

[32] J. Liang, Y. Jiao, M. Jaroniec, S. Z. Qiao, *Angew. Chemie Int. Ed.* **2012**, *51*, 11496–11500.

[33] Y. Hori, *Mod. Asp. Electrochem.* **2008**, 89–189.

[34] Y. Hori, H. Wakebe, T. Tsukamoto, O. Koga, *Electrochim. Acta* **1994**, *39*, 1833–1839.

[35] T. J. Bandosz, M. Seredych, E. Rodríguez-Castellón, Y. Cheng, L. L. Daemen, A. J. Ramírez-Cuesta, *Carbon.* **2016**, *96*, 856–863.

[36] M. Seredych, E. Rodríguez-Castellón, T. J. Bandosz, *Carbon* **2016**, *107*, 501–509.

[37] M. Seredych, J. Jagiello, T. J. Bandosz, *Carbon N. Y.* **2014**, *74*, 207–217.

[38] J. S. Duchene, G. Tagliabue, A. J. Welch, W. H. Cheng, H. A. Atwater, *Nano Lett.* **2018**, *18*, 2545–2550.

[39] S. Aoi, K. Mase, K. Ohkubo, T. Suenobu, S. Fukuzumi, *ACS Energy Lett.* **2017**, *2*, 532–536.

[40] Y. Nakabayashi, Y. Hirano, Y. Sakurai, A. Okazaki, H. Kuriyama, N. Roy, N. Suzuki, K. Nakata, K. ichi Katsumata, A. Fujishima, et al., *J. Appl. Electrochem.* **2018**, *48*, 61–73.

[41] C. W. Li, M. W. Kanan, *J. Am. Chem. Soc.* **2012**, *134*, 7231–7234.

[42] H. Tong, Y. Jiang, Q. Zhang, J. Li, W. Jiang, D. Zhang, N. Li, L. Xia, *ChemSusChem*

2017, *10*, 3268–3275.

[43] S. Wang, L. Zhao, L. Bai, J. Yan, Q. Jiang, J. Lian, *J. Mater. Chem. A* **2014**, *2*, 7439–7445.

[44] J. Robertson, E. P. O'Reilly, *Phys. Rev. B. Condens. Matter* **1987**, *35*, 2946–2957.

[45] J. Jagiello, J. P. Olivier, *Adsorption* **2013**, *19*, 777–783.

[46] J. Jagiello, J. P. Olivier, *Carbon.***2013**, *55*, 70–80.

[47] J. Jagiello, T. J. Bandosz, J. A. Schwarz, Carbon **1992**, *30*, 63–69.

[48] M. Seredych, S. Łos, D. A. Giannakoudakis, E. Rodríguez-Castellón, T. J. Bandosz, *ChemSusChem* **2016**, *9*, 795–799.

[49] M. Radecka, M. Rekas, A. Trenczek-Zajac, K. Zakrzewska, *J. Power Sources* **2008**, *181*, 46–55.

10.1002/cssc.201801073

The table of contents entry

FULL PAPER

On S, N codoped nanoporous carbons, upon irradiation, photocurrent was generated during CO_2 reduction process. Thiophenic sulfur contributes to sample's photoactivity in visible light. These species enhance the overall reduction process promoting both hydrogen evolution reaction and CO_2 reduction to CO. Porosity was also found as an important factor.

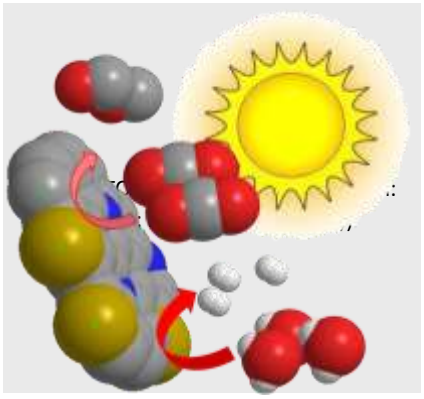

*Author(s), Corresponding Author(s)**
*Wanlu Li and Teresa J. Bandosz**

Role of heteroatoms in S, N-codoped nanoporous carbons in CO_2 (photo)electrochemical reduction